Sensors & Actuators: B. Chemical 284 (2019) 110–117

Contents lists available at ScienceDirect

Sensors and Actuators B: Chemical

journal homepage: www.elsevier.com/locate/snb

Mixed-potential type triethylamine sensor based on NASICON utilizing $SmMO_3$ (M = Al, Cr, Co) sensing electrodes

Ce Ma, Liwei Wang, Yueying Zhang, Xinyu Yang, Xishuang Liang*, Xidong Hao, Tong Liu, Fangmeng Liu, Xu Yan, Yuan Gao, Peng Sun, Geyu Lu*

State Key Laboratory on Integrated Optoelectronics, Jilin Province Key Laboratory on Gas Sensors, College of Electronic Science and Engineering, Jilin University, 2699 Qianjin Street, Changchun, 130012, China

ARTICLE INFO

Keywords:
NASICON
Triethylamine gas sensor
Perovskite
Mixed potential

ABSTRACT

The polycrystalline perovskite $SmMO_3$ (M = Al, Cr, Co) sensing electrode was synthesized by the sol-gel method, and the NASICON-based sensors attached with $SmMO_3$ were designed and fabricated for triethylamine (TEA) detection. This study investigated the effects of different M^{3+} ions in $SmMO_3$ and various calcination temperatures of the sensing material on TEA sensing properties. The results reveal that compared with the other devices, the sensor attached with $SmCrO_3$ sintered at 800 °C displays a higher response value (−108.2 mV) towards 100 ppm TEA, and that the sensor even detects 2 ppm TEA with an acceptable value (−6 mV). The sensor utilizing $SmCrO_3$ (800 °C) also exhibits pretty swift response and recovery times of 2 and 22 s, respectively, toward 20 ppm TEA. A linear relationship exists between the response values and the logarithm of TEA concentrations, and the sensitivity is −64 mV/decade. At the same time, good repeatability, selectivity, and long-term stability of the sensor are also observed. Furthermore, the sensing mechanism related to the mixed potential model is demonstrated by the polarization curve measurements.

1. Introduction

Triethylamine (TEA), a colorless transparent liquid with a strong fishy malodor, is one of the most noteworthy organic amines and has been widely used as catalyst, preservative, organic solvent and synthetic dye [1]. Under natural conditions, TEA is typically extracted from wastewater, dead fish and other sea creatures, and its concentration increases significantly with the prolonged decomposition time of dead marine products [2]. Considering the intense volatility, inflammability and toxicity of TEA, more attention should be put into this dangerous organic compound. An explosive mixture emerges once the TEA steam mixes with air, and this perilous event is aggravated when the mixture gas is exposed to a naked flame [3]. In addition, TEA negatively affects human health. TEA can induce skin burns, ocular irritation and respiratory difficulty to individuals commonly exposed to TEA. Moreover, long-term continuous exposure to TEA can even lead to abnormal embryonic development [2]. OSHA (Occupational Safety and Health Administration) stipulated that the TEA concentration in air should be under 10 ppm on a volumetric basis (ppmV) to avoid the potential health risk [4,5]. It is urgent to develop highly sensitive TEA sensor for the biomedicine, chemical industries and sea food detection due to the hazards imposed by TEA on human health and the living environment.

Currently, there are several TEA detection methods available, including chromatography [6,7], electrochemistry analysis [8,9] and colorimetric method [10]. These detection methods have demonstrated their outstanding sensing properties. However, the expensive equipment and complex manipulation restrict their extensive application. Thus, a reliable and convenient gas sensor aiming at the real-time TEA monitoring is urgently demanded for practical application. Fortunately, the solid-electrolyte-type gas sensors featuring miniaturization, good cross-selectivity and steady sensing properties, have been regarded as the most written topic for hazardous gas detection. Among various solid electrolytes, NASICON (sodium super ionic conductor) presents a high ionic conductivity between 200 °C and 500 °C and has attracted the attention of numerous researchers. The NASICON-based sensors usually work at the intermediate temperature zone and the low working temperature means fewer operating costs [11]. NASICON-based gas sensors have been developed to monitor multifarious hazard gases, including Cl_2 [12,13], H_2S [14], SO_2 [15,16], NH_3 [17] and VOCs [2,18]. Although this type of sensor has a wide monitoring scope for toxic gas, however, few researchers explored the application of NASICON-based gas sensors for TEA monitoring in the past several decades. Thus,

* Corresponding authors.
E-mail addresses: liangxs@jlu.edu.cn (X. Liang), lugy@jlu.edu.cn (G. Lu).

https://doi.org/10.1016/j.snb.2018.12.108
Received 12 March 2018; Received in revised form 18 December 2018; Accepted 20 December 2018
Available online 21 December 2018

developing a NASICON-based gas sensor for TEA detection was thought of as a meaningful task.

The sensing performance of the NASICON-based sensor was strongly affected by the electrochemical catalytic activity of electrode toward the target gas. Therefore, choosing and exploiting the appropriate SE is considered to be a research emphasis. To date, the perovskite composite oxides, one of the most important electrocatalytic materials, have been developed as sensing materials for the gas sensor at both high and intermediate working temperatures [19–21]. For the mixed-potential-type gas sensor, the different elementary compositions in A-site or B-site play a vital role in gas sensing characteristic for the sensing electrode [22–24]. As a Sm-based perovskite, $SmCrO_3$ has been investigated in the magnetometric property [25–27]. Maike Siemons et al. synthesized $SmCrO_3$ by the polyol-mediated method to measure its conductance and sensing properties toward H_2, CO and NO_x [28]. As of today, there are still no reports about the application of $SmCrO_3$ in TEA detection. In this study, we fabricated the NASICON-based gas sensor utilizing $SmMO_3$-SE (M = Al, Cr, Co) prepared by a facile sol-gel method, and compared the sensing characteristics of different sensing materials toward TEA detection. Furthermore, more sensing properties of the sensors were systematically measured and the sensing mechanism was discussed.

2. Experimental

2.1. Preparation of the electrolyte and sensing materials

All the reagents in this experiment were of analytical-grade purity (Beijing Chemicals Co. Ltd.) and used as received without any further purification.

Solid-state electrolyte NASICON ($Na_3Zr_2Si_2PO_{12}$, x = 2) powder was synthesized by the sol-gel method. In the synthesis process of NASICON, $ZrO(NO_3)_2{\cdot}8H_2O$, $NaNO_3$, $(NH_4)_2HPO_4$ and $Si(C_2H_5O)_4$ were used as the raw materials. First, $Si(C_2H_5O)_4$ was mixed with the deionized water and ethanol at a specific volume proportion (1:0.717:1). It was stirred at 50 °C for 1 h until a transparent solution was formed. After that, the mixture was dropped into the prepared $ZrO(NO_3)_2{\cdot}8H_2O$ solution and stirred at 80 °C for 30 min, and $NaNO_3$ solution and $(NH_4)_2HPO_4$ solution were added in the same manner. The white and viscous sol was obtained after 4 h of stirring at 80 °C. The sol was then aged and dried in the dry oven, and the obtained solid gel was pre-calcined at 400 °C for 4 h. Finally, the resultant NASICON precursor powder was pressed into the pellets and sintered at 900 °C for 9 h to obtain the NASICON powder.

$SmCrO_3$ powder was successfully prepared by the sol-gel method. In a typical procedure, 2.2225 g $Sm(NO_3)_3{\cdot}6H_2O$ (samarium nitrate hexahydrate) and 2 g $Cr(NO_3)_3{\cdot}9H_2O$ (chromic nitrate nonahydrate) were mixed in 20 ml deionized water according to the certain proportion (n(Cr^{3+}): n(Sm^{3+}) = 1:1) and continuously stirred until both salts were completely dissolved. 6.3 g Citric acid (CA) was simultaneously dissolved in 20 ml deionized water at a fixed stoichiometric quantity. The CA solution was then added into the mixed nitrate solution and the obtained mixture was stirred at 80 °C. After a green gel formed, the product was placed in the drying oven to eliminate any residuary water. Subsequently, the obtained xerogel precursor was pre-calcined at 400 °C for 4 h. Finally, the products were sintered at different calcination temperatures (700 °C, 800 °C, 900 °C) for 2 h to obtain $SmCrO_3$ powders. In addition, $SmMO_3$ (M = Al and Co) sensing materials were also prepared using the same procedure.

2.2. Sample characterization and sensing performance tests of gas sensor

The elementary composition and the crystal phase of $SmMO_3$ (M = Al, Cr, Co) were analyzed by Rigaku wide-angle X-ray powder diffraction (XRD, D/max rA, using Cu Kα radiation at wave length = 0.1541 nm) at the range of 20°–80°. Field-emission scanning electron microscopy (FESEM, JEOL JSM-7500F, with an accelerating voltage of 15 kV) was used to observe the grain size and morphology of the samples.

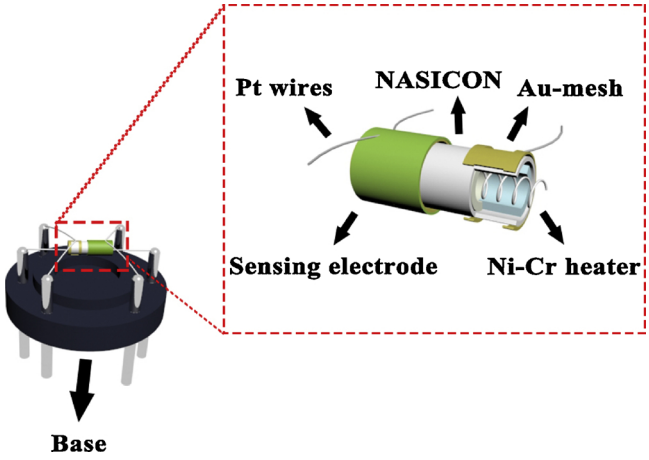

Fig. 1. Schematic diagram of the present gas sensor.

The structure of the sensor using the alumina tube is shown in Fig. 1. 0.5 g NASICON powder was mixed with a minimum quantity of deionized water (about 0.5 ml). After 20 min's grinding in the agate mortar, the resultant paste was covered on the clean alumina tube surface by a fine brush to form a smooth NASICON film. The above-mentioned process was repeated twice to ensure the thickness (about 0.5 mm) of NASICON film.

Subsequently, the tube with NASICON layer was pre-calcined at 600 °C for 1 h, and then calcined at 900 °C for 6 h. By applying commercial gold ink, several narrow ring-shaped Au electrodes were connected and manually formed on two ends of the NASICON thick film using a small brush. Pt wire was attached to the Au electrode as the lead wire. Then, the tube was sintered at 800 °C for 30 min. After one end of the ring-shaped Au electrode was covered with $SmMO_3$ paste, the sensor was sintered at 600 °C for 4 h. Finally, a Ni−Cr alloy coil was introduced as a heater into the alumina tube so that the operating temperature could be controlled by adjusting the heating current. The gas sensing properties of the fabricated sensor were measured according to a conventional static method [29], and the sensing signal was recorded by a computer linked with a digital electrometer (Rigol Technologies, Inc, DM3058, China). The electrochemical impendence curves were measured by an electrochemical interface and impedance/gain phase analyzer (Solartron SI 1287 and SI 1260). The different concentrations of target gases were prepared by the static liquid gas distribution method. A certain amount of TEA or other solvents were injected into the chamber via a special airlock at side of the chamber using a microsyringe, and the ventilators in the chamber worked quickly to evenly distribute the test gases in the chamber. The concentrations of target gas were calculated using the following formula.

$$C = \frac{22.4 * \rho * \varphi * V_1}{M * V_2}$$

Here, C (ppm) is the target gas TEA concentration; ρ (g/mL) is the liquid density; φ is the required gas volume fraction; V_1(μL) and V_2(μL) are the volumes of the liquid and the chamber, respectively; and M (g/mol) is the molecular weight of the liquid [33]. The polarization curves at the range of 0 mV to −120 mV were carried out by an electrochemical workstation (CHI600C, Instrument corporation of Shanghai, China) measuring in the different concentrations of target gas.

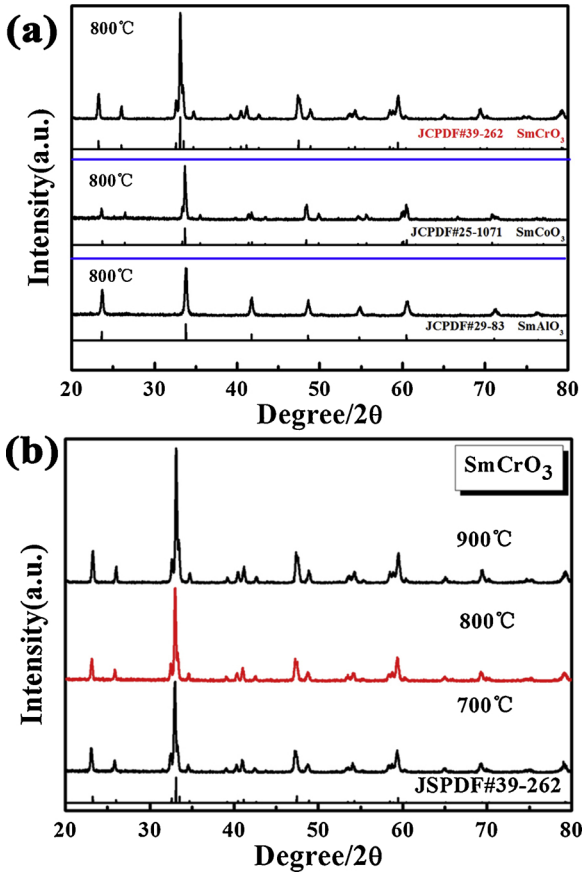

Fig. 2. (a) XRD pattern of synthesized $SmMO_3$ (M = Cr, Co, Al) sintered at 800 °C; (b) XRD pattern of $SmCrO_3$ sintered at different temperature (700 °C, 800 °C, 900 °C).

3. Results and discussion

3.1. Characteristics of the sensing materials

To confirm the elementary composition and crystalline phase of synthesized products $SmMO_3$ (M = Al, Cr, Co), X-ray diffraction (XRD) was performed and the result is displayed in Fig. 2. Fig. 2(a) displays the XRD patterns of the $SmMO_3$ (M = Al, Cr, Co) sintered at 800 °C. The obtained $SmAlO_3$, $SmCoO_3$ and $SmCrO_3$ are in accordance with JCPDS PDFs (#29–83, #25–1071 and #39–262) without any impurity peaks. All the obtained products are assigned as the orthorhombic structure and exhibit the sharp reflection peaks. The XRD patterns of $SmCrO_3$ powder sintered at different temperatures (700 °C, 800 °C, 900 °C) are exhibited in Fig. 2(b). The reflection peaks become sharper with the increased calcination temperature, suggesting that the crystallinity of the samples is improved at higher sintering temperatures.

The grain sizes and surface microstructures of the sensing electrode materials are shown in Fig. 3. Fig. 3(a–c) display the SEM images of $SmMO_3$ (M = Al, Co, Cr) sintered at 800 °C. The morphologies of the synthesized sensing materials contain numerous particles with equal size and reveal a porous structure. The porous structure of SE is beneficial for the proposed sensor, because it promotes the convenient gas diffusion process when TEA molecules pass through the sensing material. The SEM images of $SmCrO_3$ sintered at different temperatures are exhibited in Fig. 3(c–e). The grain size of the sensing material calcined at the higher temperature remains larger. The sensing material $SmCrO_3$ sintered at 800 °C has a better porosity than that of $SmCrO_3$ sintered at other temperatures (700 °C and 900 °C) according to the SEM images.

3.2. Sensing performances of the sensors

To investigate the effect of different B-site elements on the gas sensing characteristic, the sensor utilizing $SmMO_3$ (M = Al, Cr, Co) sintered at 800 °C was measured toward 100 ppm TEA, and the result is displayed in Fig. 4(a). The sensor utilizing $SmCrO_3$-SE exhibits the highest response value (−108.2 mV) out of all the sensors. The following analysis highlighted the sensor using $SmCrO_3$-SE. The response values of the sensor using $SmCrO_3$-SE sintered at the different temperatures (700 °C, 800 °C, 900 °C) are compared in Fig. 4(b). The sensor with $SmCrO_3$ (800 °C)-SE displays a higher response value than the other two sensors. Overall, the sensor utilizing $SmCrO_3$ (800 °C)-SE exhibits the best sensing characteristic for TEA. Hence, considerable attention is paid to investigate the sensing properties of the sensor utilizing $SmCrO_3$ (800 °C)-SE.

The sensing mechanism of NASICON-based sensors using $SmMO_3$-SEs should keep in accordance with the mixed-potential theory [30,31]. Based on the mixed-potential theory, the fabricated sensor can be seen as the following electrochemical cells:

In air: O_2 in air, $SmMO_3$, Au | NASICON | Au, O_2 in air

In TEA: $(C_2H_5)_3N + O_2$, $SmMO_3$, Au | NASICON | Au, $(C_2H_5)_3N + O_2$

Anodic reaction: $2(C_2H_5)_3N + 39Na_2O \rightarrow N_2 + 78Na^+ + 12CO_2 + 15H_2O + 78e^-$ (1)

Cathodic reaction: $78Na^+ + 78e^- + 39/2O_2 \rightarrow 39Na_2O$ (in NASICON) (2)

When the sensor is exposed to the target gas, both the sensing electrode (SE) and the reference electrode (RE) are in the TEA atmosphere, and the electrochemical Reactions (1) and (2) occur simultaneously and form a local cell. In the case of the mixed-potential sensor, the dynamic balance is attained when the rates of two electrochemical reactions are identical, and the electrode potential at the SE is regarded as the mixed-potential value at this moment. The potential difference ΔV between SE and RE is recorded as the sensing signal [32].

The influence of the calcination temperature in the sensing characteristic of SE can be divided into two factors. On the one hand, the sensing material sintered at the different temperatures displays the different microstructure. According to SEM images, the sensing material $SmCrO_3$ (800 °C) has a relatively larger pore aisle, which allows TEA gas to pass through the aisle faster and avoids the loss in the gas diffusion process. This means, the sensing material with the wider pores is assumed to offer less gas molecule loss by diffusion before reaching the reaction site of mixed potential generation. On the other hand, the calcination temperature could also affect the electrochemical catalytic activity of SE. To prove this hypothesis, the polarization curve of the sensor utilizing $SmCrO_3$ sintered at the different temperatures in 100 ppm TEA was measured, and the result is exhibited in Fig. 5(a). The slope of the sensor attached with $SmCrO_3$ (800 °C)-SE is higher, and a higher slope implies a greater catalytic activity. The results indicate that the different calcination temperatures critically affected the catalytic activity of the sensing material $SmCrO_3$. Moreover, this influence is also displayed by the sensing performance of the present sensor, hence, the response value of the sensor attached with $SmCrO_3$ (800 °C) is higher than that of the rest.

B-site elements are typically a significant factor in the electrochemical catalytic activity for the perovskite-type composite oxide [27,39]. Nguyen Duc Tho et al investigated the effect of different B-site elements in the perovskite composite oxide $LaMO_3$ (M = Mn, Fe, Co, Ni) on the sensing characteristic of YSZ-based sensor toward various gases of NO_2, NO, CO, C_3H_8 and CH_4. The presence of different elements can result in the enhanced absorbed-oxygen formation reaction on the perovskite particle surface, and a weakened gas-catalytic

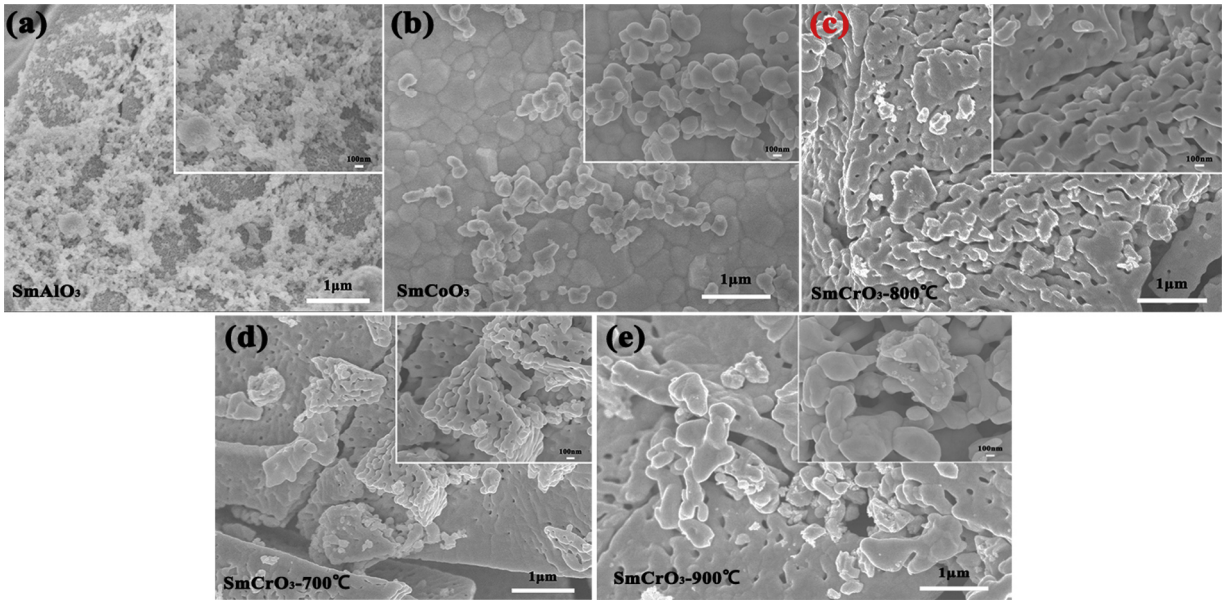

Fig. 3. SEM images of $SmMO_3$ (M = Al, Cr, Co). (a) $SmAlO_3$ sintered at 800 °C; (b) $SmCoO_3$ sintered at 800 °C; (c) $SmCrO_3$ sintered at 800 °C; (d) $SmCrO_3$ sintered at 700 °C; (e) $SmCrO_3$ sintered at 900 °C.

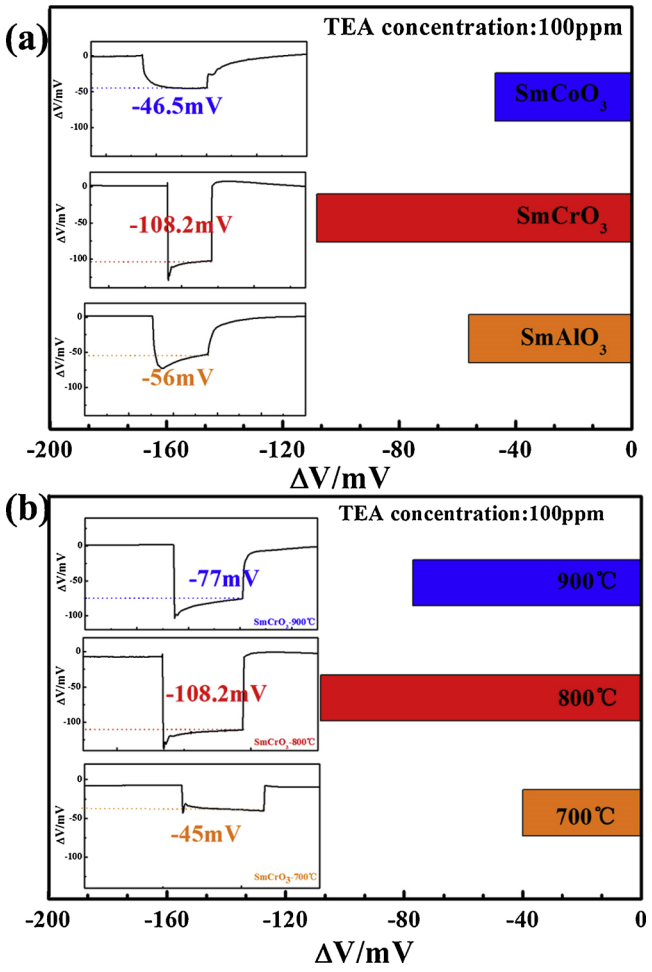

Fig. 4. (a) The response value of the sensor utilizing $SmMO_3$ (M = Al, Cr, Co) sintered at 800 °C towards 100 ppm TEA; (b) The response value of the sensor utilizing $SmCrO_3$ sintered at different temperature (700 °C, 800 °C, 900 °C) towards 100 ppm TEA.

reaction. This phenomenon could lead to the electrochemical catalytic property difference of sensing material toward the target gas. As the result, the different potential response values of the sensors were observed. To investigate the reason that the sensor using $SmCrO_3$-SE (800 °C) displayed more superior sensing properties than those of sensors using other SEs ($SmAlO_3$ and $SmCoO_3$) and validate the mixed potential mechanism, the polarization curves and complex impedance curves of the fabricated devices were measured. Fig. 5(b) compares the polarization curves of the sensor utilizing $SmMO_3$ (M = Al, Cr, Co) in the sample gas (100 ppm TEA + air). The current of the sensor using $SmCrO_3$-SE is shifted upward to higher values and shows a larger slope than that of other two sensors. As such, the sensor utilizing $SmCrO_3$-SE has the highest electrochemical catalytic activity on the whole electrochemical reaction occurring on SE. The obtained curves result from the combination effect of both the anodic electrochemical Reaction (1) and the cathodic electrochemical Reaction (2) for the present sensors. The larger slope indicates that the sensor utilizing $SmCrO_3$-SE owns the stronger catalytic property towards the sample gas. In this case, the sensor with $SmCrO_3$-SE exhibits a higher response value than those of the sensor utilizing other SEs.

To verify this result, the complex impedance curve is tested to compare the electrocatalytic performances of different sensing materials. Fig. 5(c) displays the electrochemical impedance curves of the sensors utilizing $SmMO_3$ (M = Al, Cr, Co) toward 100 ppm TEA. According to the previous reports [33,34], the resistance at a higher frequency (the smaller semicircle) is generally considered to be the interfacial charge transport resistance between the electrolyte and SE, which suggests the charge transfer speed. As for the resistance at a lower frequency 0.1 Hz (the larger semicircle), this is related to Warburg resistance resulting from the ion diffusion behavior, indicating the gas molecule diffusion speed of disparate sensing materials [35–37]. The sensor utilizing $SmCrO_3$-SE displays the smaller semicircle in both high-frequency and low-frequency regions from Fig. 5(c). This means that the sensor utilizing $SmCrO_3$-SE owns the quickest electron transport speed and gas molecule diffusion speed, resulting in the strongest electrochemical catalytic activity. This result is also consistent with the polarization curve in Fig. 5(b). The faster electron transport and gas molecule diffusion speeds lead to the enhanced electrochemical reaction process. They also demonstrate that the current curve of the sensor using $SmCrO_3$-SE owns the larger slope and reaches the higher value. At

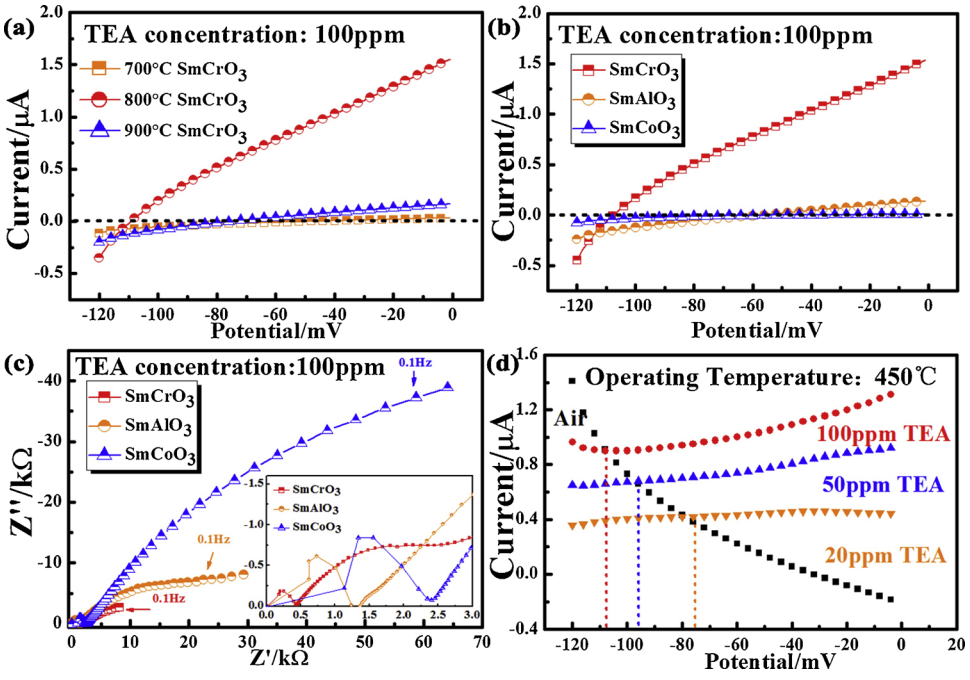

Fig. 5. (a) Polarization curves of the sensors utilizing $SmCrO_3$ sintered at different temperatures (700 °C, 800 °C, 900 °C) toward 100 ppm TEA; (b) Polarization curves of the sensors utilizing $SmMO_3$ (M = Al, Cr, Co) sintered at 800 °C toward 100 ppm TEA; (c) Electrochemical impedance curves for the sensors attached with $SmMO_3$ (M = Al, Cr, Co) toward 100 ppm TEA; (d) Polarization curves exposed to different concentrations of TEA (20, 50 and 100 ppm) and air for the sensor attached with $SmCrO_3$ sintered at 800 °C.

the same time, the semicircle size sequence is the same as the response value order of the sensors toward 100 ppm TEA. The sensing material $SmMO_3$ was prepared with the same method and condition, and different B-site elements on the chemical properties of sensing materials are investigated. For the present sensors, $SmCrO_3$ sintered at 800 °C displays a stronger catalytic activity than those of the other two kinds of sensing material. This is revealed by both the polarization curve and the complex impedance curve. Therefore, when the approximate operating condition ensures the similar kinetics process of electrochemical reactions, it was determined that B-site element Cr^{3+} promoted the catalytic activity of the perovskite $SmMO_3$, resulting in the improved sensing performance of the present sensor.

Moreover, the polarization curves of the sensor attached with $SmCrO_3$-SE were measured in atmospheres containing air and different concentrations of TEA (20, 50 and 100 ppm) and the result is shown in the Fig. 5(d). The intersection value of the cathodic curve and anodic curve was generally consistent with the response value observed in the experimental test, thereby confirming the mixed-potential mechanism. The comparison of mixed-potential estimated values and the observed values was exhibited in the practical experiment in Table 1. This reveals that both values remained nearly consistent for present sensors, further validating that the present sensor using $SmCrO_3$-SE adheres to the mixed-potential mechanism [38,39].

The operating temperature has a prominent impact on the sensing properties of the NASICON-based sensors. So the sensor attached with $SmCrO_3$ (800 °C)-SE was measured toward 100 ppm TEA at the different operating temperatures (350 °C–500 °C), as shown in Fig. 6. The

Table 1
Comparison of the mixed-potential estimated and the potential difference value observed for the sensors attached with different SEs.

Sensors	TEA Conc. (ppm)	Potential difference value (observed) (mV)	Potential difference value (estimated) (mV)
$SmAlO_3$(800 °C)-SE	100	−56	−56
$SmCoO_3$(800 °C)-SE	100	−46.5	−47
$SmCrO_3$(800 °C)-SE	100	−108.2	−107
$SmCrO_3$(800 °C)-SE	50	−94.5	−93.9
$SmCrO_3$(800 °C)-SE	20	−76.3	−78

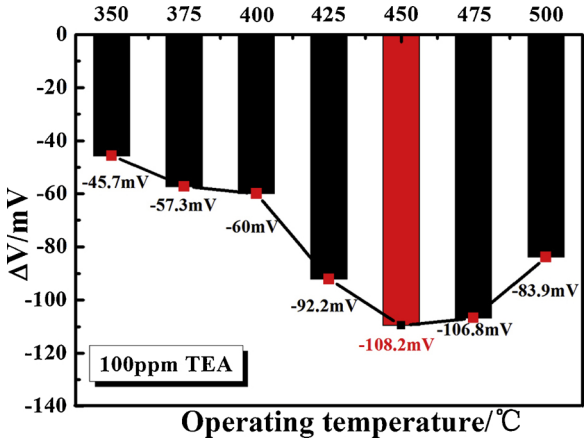

Fig. 6. The response values of the sensor attached with $SmCrO_3$ (800 °C)-SE at different operating temperatures (350 °C–500 °C).

temperature dependence behavior presents the inverted volcano-shape tendency, and the highest response value (−108.2 mV) is obtained at 450 °C. The probable reason would be set forth as follows. For the NASICON-based sensor, a sufficient energy supply must be guaranteed to achieve a smooth electrochemical reaction process. When the operating temperature is below 450 °C, the temperature is not high enough to enable high kinetics of potential forming electrochemical reactions at the given activation energy. As the operating temperature increases, the electrochemical reaction is enhanced and the improved response value is observed. However, when the temperature is beyond 450 °C, the reduced response value is observed for the present sensor. This situation is caused by two factors: physical gas desorption and the chemical oxidation process [42,43]. On the one hand, as the operating temperature increases, the TEA desorption process begins to take up the dominant position, reducing a smaller amount of TEA participating in the electrochemical reaction. Consequently, the potential forming reaction was weakened. On the other hand, the higher operating temperature can result in a more violent chemical oxidation reaction for TEA gas in the diffusion process. The gas loss from the transport process is also responsible for the reduced electrochemical reactions. Finally, both factors lead to the TEA gas loss and reduce the electrochemical

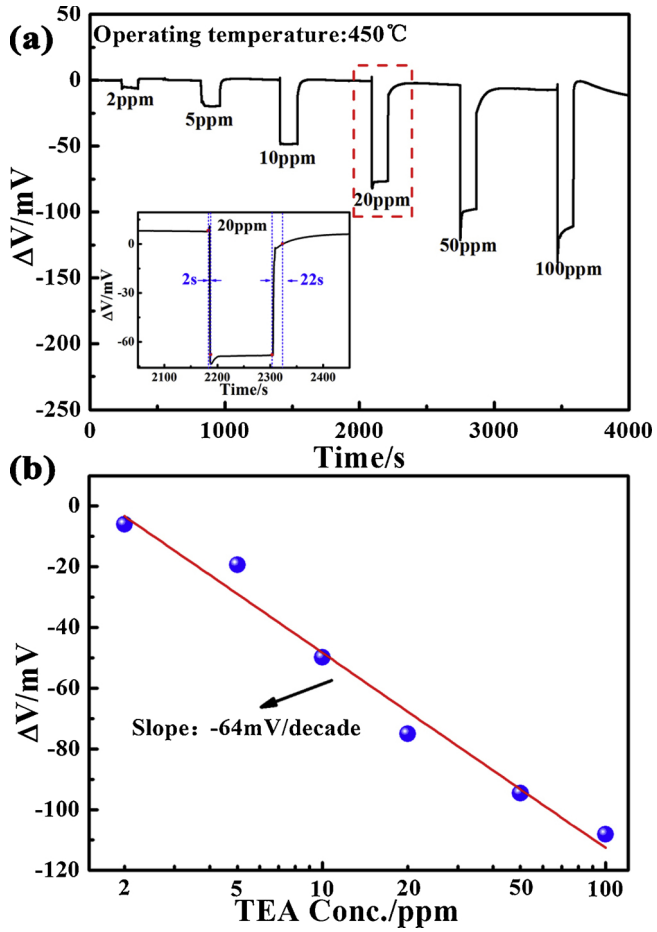

Fig. 7. (a) The response and recovery transient curves for the sensor utilizing $SmCrO_3$ (800 °C)-SE towards different concentrations of TEA at the range of 2–100 ppm at 450 °C and the response and recovery speed at 20 ppm TEA (inset). (b) Dependence of ΔV on logarithm of TEA concentrations at the range of 2–100 ppm for the sensor attached with $SmCrO_3$ (800 °C)-SE.

Table 2
Comparison of the sensing performance of the present sensor and that of devices reported in literatures.

Sensing material	TEA Conc. (ppm)	Response value	Low detection (ppm)	Refs.
$SmCrO_3$	100	−108.2 mV	2	This work
ZnO micropyramids	50	45(R_a/R_g)	2	[41]
Zn_2SnO_4	100	37(R_a/R_g)	5	[41]
$ZnFe_2O_4$/α-Fe_2O_3	100	42.4 (R_a/R_g)	30	[44]
Zn-doped In_2O_3	50	36 (R_a/R_g)	5	[45]
α-Fe_2O_3 microrod	500	41.9 (R_a/R_g)	20	[46]
polyaniline hybrid	100	69 (R_a/R_g)	10	[47]
NiO/SnO_2 hollow sphere	10	48.6 (R_a/R_g)	2	[48]
$NiMoO_4$	100	−85mV	0.1	[49]

reaction, thus the response value of the sensor toward TEA is once again decreased. At 450 °C, both the demanded energy and TEA adhering amount for the reaction process achieve a balance so that the highest response value of the fabricated sensor is observed. In conclusion, 450 °C is considered to be the optimal operating temperature and all the subsequent sensing performance tests of the sensor with $SmCrO_3$-SE (800 °C) would be operated at 450 °C.

To explore the detailed sensing properties of the sensor with $SmCrO_3$ (800 °C)-SE in detail, the response and recovery transient

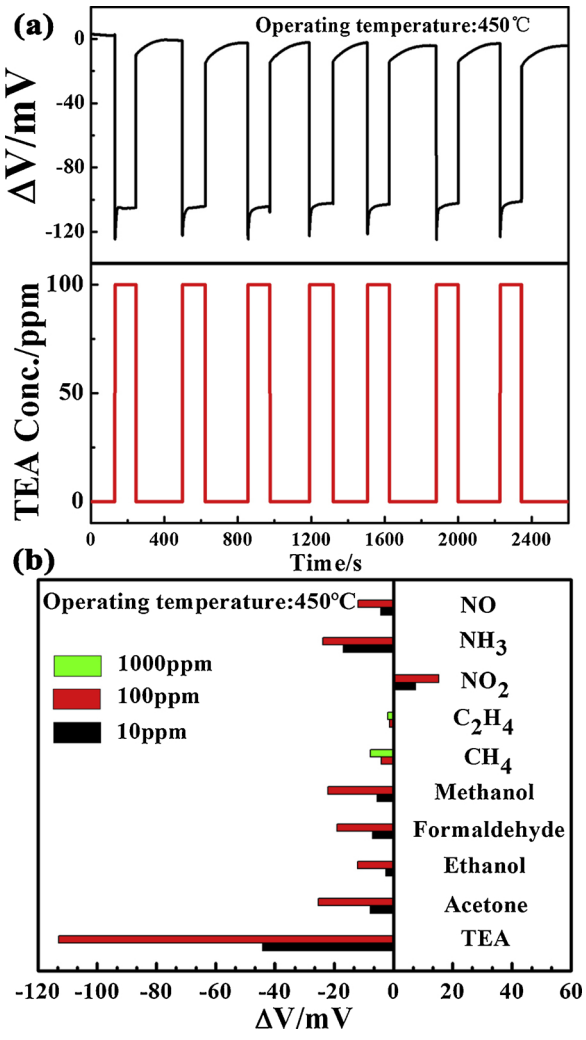

Fig. 8. (a) Continuous response-recovery transient curves towards 100 ppm TEA for the sensor attached with $SmCrO_3$ (800 °C). (b) The cross-sensitivities of the sensor utilizing $SmCrO_3$-SE to different concentrations of various gases at 450 °C.

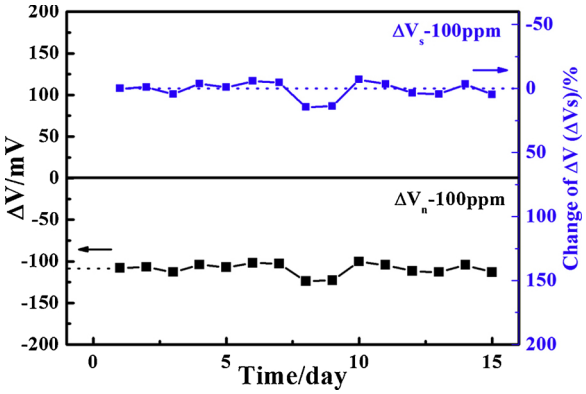

Fig. 9. Long-term stability of the sensor attached with $SmCrO_3$ (800 °C) towards 100 ppm TEA during 15 days.

curves were examined during 2–100 ppm TEA, as shown in Fig. 7(a). The same measurement time was maintained in every testing condition including air and various concentrations of TEA. The response signals in the TEA atmosphere at the final time marking were recorded to ensure accuracy. The response signals of the sensor changed quickly upon switching on- and off-TEA at 450 °C, indicating a swift response and

recovery rate. When the sensor was exposed to 20 ppm TEA, the 90% response and recovery times were approximately 2 and 22 s, respectively. The response value ΔV of the sensor toward 100 ppm TEA reaches as high as -108.2 mV. Even toward 2 ppm TEA, the response value of the present sensor can still reach −6 mV, indicating the sensor can detect the low concentrations of TEA. Fig. 7(b) shows that the sensitivity almost linearly depends on the logarithm of TEA concentration in the range of 2–100 ppm for the present sensor, and a slope of −64 mV/decade is achieved. This linear relationship is confirmed to be consistent with the mixed-potential mechanism [40]. The sensing properties between the fabricated sensor and the sensors reported in the previous literature are listed in Table 2. The response value unit of the mixed-potential type sensor is given in mV, and the sensitivity of the metal-oxide-semiconductor type gas sensor is recorded as S ($S = R_a/R_g$, R_a is resistance of the sensor in the air, R_g is the resistance of the sensor in the target gas). The fabricated sensor displays a good detectability for the TEA gas with a pretty low detection limit (2 ppm). These characteristics illustrate that the present sensor has a promising prospect in the TEA detection.

Seven testing cycles of repeatable response-recovery transient from the present sensor were measured toward 100 ppm TEA at 450 °C. As shown in Fig. 8(a), the response signal is effectively reproduced and the response value change is insignificant. The maximum response value change is only 4 mV, signifying the repeatability potential of the fabricated sensor. Moreover, the cross-selectivity toward different concentrations of interfering gas is measured for the present sensor in Fig. 8(b). Various gases including NO_x, NH_3 and acetone at the specific concentrations (10 ppm and 100 ppm) are tested under the same test condition. The fabricated sensor exhibits the higher response values toward TEA than other interfering gases at both 100 ppm and 10 ppm. Overall, the present sensor displays good selectivity toward most interfering gases.

To quantitatively elucidate the change amplitude of ΔV during the 15 days operating period, the long-term stability of the present sensor was measured toward 100 ppm TEA during 15 days, and the change rate of response value called ΔV_s is calculated according to the equation $\Delta V_s = (\Delta V_n - \Delta V_1)/\Delta V_1 \times 100\%$ (ΔV_1 is the response value of the present sensor on the first day, and ΔV_n is on behalf of the response value on the nth day). As shown in Fig. 9, the response values of the fabricated sensor toward 100 ppm TEA remain consistent, and the result indicates that ΔV_s is under 15% from beginning to end. This slight change shows consistency of the transients, and the present sensor shows great stability over the period of 15 days.

4. Conclusion

The NASICON-based sensors utilizing $SmMO_3$-SE (M = Al, Cr, Co) prepared by the sol-gel method are fabricated and investigated aiming at TEA detection. The effects of different B-site elements and different calcination temperatures of the sensing material on sensing properties were assessed. The result indicates that the sensor attached with $SmCrO_3$ (800 °C)-SE displays the highest response value toward 100 ppm TEA, and a fast response and recovery rate toward 20 ppm TEA along with good sensitivity to TEA concentration at the ranges of 2–100 ppm. The detection limit can even reach 2 ppm.In addition, the present sensor also shows excellent repeatability, long-term stability and selectivity against various interfering gases. Overall, the sensor utilizing $SmCrO_3$ (800 °C)-SE exhibits the potential application value for TEA detection.

Acknowledgements

This work was supported by the National Nature Science Foundation of China (Nos. 61473132, 61533021 and 61520106003), National Key R&D Program of China (No. 2016YFC0201002) and Program for Chang Jiang Scholars and Innovative Research Team in University (No. IRT-17R47), Application and Basic Research of Jilin Province (20130102010JC), STIRT-JLU (2017TD-07).

References

[1] W. Li, H. Xu, T. Zhai, H. Yu, Q. Xu, X. Song, et al., High-sensitivity, high-selectivity, and fast-recovery-speed triethylamine sensor based on ZnO micropyramids prepared by molten salt growth method, J. Alloys Compd. 695 (2017) 2930–2936.
[2] F. Liu, X. Yang, B. Wang, Y. Guan, X. Liang, P. Sun, et al., High performance mixed potential type acetone sensor based on stabilized zirconia and $NiNb_2O_6$ sensing electrode, Sens. Actuators B Chem. 229 (2016) 200–208.
[3] H. Xu, J. Ju, W. Li, J. Zhang, J. Wang, B. Cao, Superior triethylamine-sensing properties based on TiO_2/SnO_2 n–n heterojunction nanosheets directly grown on ceramic tubes, Sens. Actuators B Chem. 228 (2016) 634–642.
[4] D. Ju, H. Xu, Z. Qiu, J. Guo, J. Zhang, B. Cao, Highly sensitive and selective triethylamine-sensing properties of nanosheets directly grown on ceramic tube by forming NiO/ZnO PN heterojunction, Sens. Actuators B Chem. 200 (2014) 288–296.
[5] T. Cai, L. Chen, Q. Ren, S. Cai, J. Zhang, The biodegradation pathway of triethylamine and its biodegradation by immobilized Arthrobacter protophormiae cells, J. Hazard. Mater. 186 (2011) 59–66.
[6] B. Gandu, K. Sandhya, A. Gangagni Rao, Y.V. Swamy, Gas phase bio-filter for the removal of triethylamine (TEA) from air: microbial diversity analysis with reference to design parameters, Bioresour. Technol. 139 (2013) 155–160.
[7] W. Li, H. Xu, T. Zhai, H. Yu, Z. Chen, Z. Qiu, et al., Enhanced triethylamine sensing properties by designing $Au@SnO_2/MoS_2$ nanostructure directly on alumina tubes, Sens. Actuators B Chem. 253 (2017) 97–107.
[8] J.F. Haskin, G.W. Warren, L.J. Priestley, Gas chromatography. Determination of constituents in study of azeotropes, Anal. Chem. 30 (1958) 2.
[9] N. Lenca, C.F. Poole, System map for the ionic liquid stationary phase tri(tripropylphosphoniumhexanamido)trimethylamine bis(trifluoromethylsulfonyl)imide for gas chromatography, J. Chromatogr. A 1524 (2017) 210–214.
[10] W.M. Moore, R.J. Edwards, L.T. Bavda, An improved capillary gas chromatography method for triethylamine. Application to sarafloxacin hydrochloride and GnRH residual solvents testing, Anal. Lett. 32 (1999) 2603–2612.
[11] P.V. Suneesh, T.G. Satheesh Babu, T. Ramachandran, Electrodeposition of aluminium and aluminium-copper alloys from a room temperature ionic liquid electrolyte containing aluminium chloride and triethylamine hydrochloride, Int. J. Miner. Metall. Mater. 20 (2013) 909–916.
[12] W.-H. Zhang, W.-D. Zhang, Fabrication of SnO_2–ZnO nanocomposite sensor for selective sensing of trimethylamine and the freshness of fishes, Sens. Actuators B Chem. 134 (2008) 403–408.
[13] Y. Yang, C.-C. Liu, Development of a NASICON-based amperometric carbon dioxide sensor, Sens. Actuators B Chem. 62 (2000) 4.
[14] H. Zhang, J. Li, H. Zhang, X. Liang, C. Yin, Q. Diao, et al., NASICON-based potentiometric Cl_2 sensor combining NASICON with Cr_2O_3 sensing electrode, Sens. Actuators B Chem. 180 (2013) 66–70.
[15] H. Zhang, X. Cheng, R. Sun, Y. Guan, Y. Liu, C. Yin, et al., Enhanced chlorine sensing performance of the sensor based NAISCON and Cr-series spinel-type oxide electrode with aging treatment, Sens. Actuators B Chem. 198 (2014) 26–32.
[16] X. Liang, Y. He, F. Liu, B. Wang, T. Zhong, B. Quan, et al., Solid-state potentiometric H_2S sensor combining NASICON with Pr_6O_{11}-doped SnO_2 electrode, Sens. Actuators B Chem. 125 (2007) 544–549.
[17] C. Ma, X. Hao, X. Yang, X. Liang, F. Liu, T. Liu, et al., Sub-ppb SO_2 gas sensor based on NASICON and $La_xSm_{1-x}FeO_3$ sensing electrode, Sens. Actuators B Chem. 256 (2018) 648–655.
[18] X. Liang, T. Zhong, B. Quan, B. Wang, H. Guan, Solid-state potentiometric SO_2 sensor combining NASICON with V_2O_5-doped TiO_2 electrode, Sens. Actuators B Chem. 134 (2008) 25–30.
[19] X. Liang, T. Zhong, H. Guan, F. Liu, G. Lu, B. Quan, Ammonia sensor based on NASICON and Cr_2O_3 electrode, Sens. Actuators B Chem. 136 (2009) 479–483.
[20] H. Zhang, C. Yin, Y. Guan, X. Cheng, X. Liang, G. Lu, NASICON-based acetone sensor using three-dimensional three-phase boundary and Cr-based spinel oxide sensing electrode, Solid State Ionics 262 (2014) 283–287.
[21] X. Liang, G. Lu, T. Zhong, F. Liu, B. Quan, New type of ammonia/toluene sensor combining NASICON with a couple of oxide electrodes, Sens. Actuators B Chem. 150 (2010) 355–359.
[22] L. Ma, S.Y. Ma, X.F. Shen, T.T. Wang, X.H. Jiang, Q. Chen, et al., $PrFeO_3$ hollow nanofibers as a highly efficient gas sensor for acetone detection, Sens. Actuators B Chem. 255 (2018) 2546–2554.
[23] H. Ikeda, A. Iio, S.A. Anggraini, N. Miura, Impedancemetric YSZ-based oxygen sensor using $BaFeO_3$ sensing-electrode, Sens. Actuators B Chem. 243 (2017) 279–282.
[24] R.P. Patil, P.V. More, G.H. Jain, P.K. Khanna, V.B. Gaikwad, $BaTiO_3$ nanostructures for H_2S gas sensor: influence of band-gap, size and shape on sensing mechanism, Vacuum 146 (2017) 455–461.
[25] H. Aono, E. Traversa, M. Sakamoto, Y. Sadaoka, Crystallographic characterization and NO_2 gas sensing property of $LnFeO_3$ prepared by thermal decomposition of LnFe hexacyanocomplexes, $Ln[Fe(CN)_6]\cdot nH_2O$, Ln = La, Nd, Sm, Gd, and Dy, Sens. Actuators B Chem. 94 (2003) 132–139.
[26] H.T. Giang, H.T. Duy, P.Q. Ngan, G.H. Thai, D.T.A. Thu, D.T. Thu, et al., Hydrocarbon gas sensing of nano-crystalline perovskite oxides $LnFeO_3$ (Ln = La, Nd and Sm), Sens. Actuators B Chem. 158 (2011) 246–251.
[27] W. Haron, A. Wisitsoraat, S. Wongnawa, Nanostructured perovskite oxides-$LaMO_3$ (M = Al, Co, Fe) prepared by co-precipitation method and their ethanol-sensing

characteristics, Ceram. Int. 43 (2017) 5032–5040.
[28] M. Tripathi, R.J. Choudhary, D.M. Phase, T. Chatterji, H.E. Fischer, Evolution of magnetic phases in $SmCrO_3$: a neutron diffraction and magnetometric study, Phys. Rev. B 96 (2017).
[29] H. Ullah, G. Murtaza, R. Khenata, S. Mohammad, A. Manzar, S.B. Omran, et al., Mechanical, electronic and magnetic properties of Sm-based perovskite-type oxides $SmMO_3$ (M = V, Fe and Co): an ab initio study, Indian J. Phys. 89 (2015) 1133–1142.
[30] S. Wang, K. Huang, C. Hou, L. Yuan, X. Wu, D. Lu, Low temperature hydrothermal synthesis, structure and magnetic properties of $RECrO_3$ (RE = La, Pr, Nd, Sm), Dalton Trans. 44 (2015) 17201–17208.
[31] M. Siemons, A. Leifert, U. Simon, Preparation and gas sensing characteristics of nanoparticulate p-type semiconducting $LnFeO_3$ and $LnCrO_3$ materials, Adv. Funct. Mater. 17 (2007) 2189–2197.
[32] Y. Guan, C. Yin, X. Cheng, X. Liang, Q. Diao, H. Zhang, et al., Sub-ppm H2S sensor based on YSZ and hollow balls $NiMn_2O_4$ sensing electrode, Sens. Actuators B Chem. 193 (2014) 501–508.
[33] H. Fan, Y. Zeng, H. Yang, X. Zheng, L. Liu, T. Zhang, Preparation and gas sensitive properties of ZnO–CuO nanocomposites, Acta Phys. Chem. Sin. 24 (2008) 1292–1296.
[34] N. Miura, J. Wang, M. Nakatou, P. Elumalai, S. Zhuiykov, M. Hasei, High-temperature operating characteristics of mixed-potential-type NO_2 sensor based on stabilized-zirconia tube and NiO sensing electrode, Sens. Actuators B Chem. 114 (2006) 903–909.
[35] Q. Liu, J. Bao, M. Yang, X. Wang, S. Lan, C. Hou, et al., A core-shell MWCNT@rGONR heterostructure modified glassy carbon electrode for ultrasensitive electrochemical detection of glutathione, Sens. Actuators B Chem. 274 (2018) 433–440.
[36] H. Zhang, J. Yi, X. Jiang, Fast Response, Highly sensitive and selective mixed-potential H_2 sensor based on (La, Sr)(Cr, Fe)O_3-delta perovskite sensing electrode, ACS Appl. Mater. Interfaces 9 (2017) 17218–17225.
[37] L. Liu, Y. Wang, Q. Meng, B. Cao, A novel hierarchical graphene/polyaniline hollow microsphere as electrode material for supercapacitor applications, J. Mater. Sci. 52 (2017) 7969–7983.
[38] H. Zhang, T. Zhong, R. Sun, X. Liang, G. Lu, Sub-ppm H_2S sensor based on NASICON and $CoCr_{2-x}Mn_xO_4$ sensing electrode, RSC Adv. 98 (2014) 6.
[39] G. Lu, N. Miura, N. Yamazoe, High-temperature sensors for NO and NO_2 based on stabilized zirconia and spinel-type oxide electrodes, J. Mater. Chem. 7 (1997) 1445–1449.
[40] M. Stranzenbach, E. Gramckow, B. Saruhan, Planar, impedance-metric NO_x-sensor with spinel-type SE for high temperature applications, Sens. Actuators B Chem. 127 (2007) 224–230.
[41] H. Jin, M. Breedon, N. Miura, Sensing behavior of YSZ-based amperometric NO_2 sensors consisting of Mn-based reference-electrode and In_2O_3 sensing-electrode, Talanta 88 (2012) 318–323.
[42] N.D. Tho, D.V. Huong, H.T. Giang, P.Q. Ngan, G.H. Thai, D.T.A. Thu, D.T. Thu, N.T.M. Tuoi, N.N. Toan, P.D. Thang, H.N. Nhat, High temperature calcination for analyzing influence of 3d transition metals on gas sensing performance of mixed potential sensor Pt/YSZ/$LaMO_3$ (M = Mn, Fe, Co, Ni), Electrochim. Acta 190 (2016) 215–220.
[43] B. Wang, S. Yao, F. Liu, Y. Guan, X. Hao, X. Liang, et al., Fabrication of well-ordered porous array mounted with gold nanoparticles and enhanced sensing properties for mixed potential-type zirconia-based NH_3 sensor, Sens. Actuators B Chem. 243 (2017) 1083–1091.
[44] Y. Li, N. Luo, G. Sun, B. Zhang, G. Ma, H. Jin, et al., Facile synthesis of $ZnFe_2O_4$ /α-Fe_2O_3 porous microrods with enhanced TEA-sensing performance, J. Alloys Compd. 737 (2018) 255–262.
[45] X. Sun, X. Liu, X. Deng, X. Xu, Synthesis of Zn-doped In_2O_3 nano sphere architectures as a triethylamine gas sensor and photocatalytic properties, RSC Adv. 6 (2016) 89847–89854.
[46] G. Sun, H. Chen, Y. Li, G. Ma, S. Zhang, T. Jia, et al., Synthesis and triethylamine sensing properties of mesoporous α-Fe_2O_3 microrods, Mater. Lett. 178 (2016) 213–216.
[47] L. Quan, J. Sun, S. Bai, R. Luo, D. Li, A. Chen, et al., A flexible sensor based on polyaniline hybrid using ZnO as template and sensing properties to triethylamine at room temperature, Appl. Surf. Sci. 399 (2017) 583–591.
[48] D. Ju, H. Xu, Q. Xu, H. Gong, Z. Qiu, J. Guo, J. Zhang, B. Cao, High triethylamine-sensing properties of NiO/SnO_2 hollow sphere P–N heterojunction sensors, Sens. Actuators B Chem. 215 (2015) 39–44.
[49] F. Liu, J. He, Z. Yang, R. You, J. Wang, L. Zhao, Q. Wang, X. Liang, P. Sun, X. Yan, G. Lu, The mixed potential type gas sensor based on stabilized zirconia and molybdate $MMoO_4$ (M: Ni, Co and Zn) sensing electrode aiming at detecting triethylamine, Sens. Actuators B Chem. 267 (2018) 430–437.

Ce Ma received the B.Eng. degree in department of electronic science and technology in 2016. He is currently studying for his M.E. Sci. degree in College of Electronic Science and Engineering, Jilin University, China.

Liwei Wang received the BS degree in Changchun University of Science and Technology in 2014. He is currently studying for his MS degree in College of Electronic Science and Engineering, Jilin University, China.

Yueying Zhang received the B.Eng. degree in department of electronic science and technology in 2017. She is currently studying for her M.E. Sci. degree in College of Electronic Science and Engineering, Jilin University, China.

Xinyu Yang received the B.Eng. degree in department of electronic science and technology in 2017. He is currently studying for his M.E. Sci. degree in College of Electronic Science and Engineering, Jilin University, China.

Xishuang Liang received the B. Eng. degree in Department of Electronic Science and Technology in 2004. He received his Doctor's degree in College of Electronic Science and Engineering at Jilin University in 2009. Now he is a professor of Jilin University, China. His current research is solid electrolyte gas sensor.

Xidong Hao received the B.Eng. degree in department of electronic science and technology in 2016. He is currently studying for his M.E. Sci. degree in College of Electronic Science and Engineering, Jilin University, China.

Tong Liu received the B.Eng. degree in department of electronic science and technology in 2015. She is currently studying for his M.E. Sci. degree in College of Electronic Science and Engineering, Jilin University, China.

Fangmeng Liu received his PhD degree in 2017 from College of Electronic Science and Engineering, Jilin University, China. Now he is a lecturer of Jilin University, China. His current research interests include the application of functional materials and development of solid state electrochemical gas sensor and flexible device.

Xu Yan received his M.S. degree in 2013 from Nanjing Agricultural University. He joined the group of Prof. Xingguang Su at Jilin University and received his pH.D. degree in June 2017. Since then, he did postdoctoral work with Prof. Geyu Lu. Currently, his research interests mainly focus on the development of the functional nanomaterials for chem/bio sensors.

Yuan Gao received her PhD degree from Department of Analytical Chemistry at Jilin University in 2012. Now she is an associate professor in Jilin University, China. Her current research is focus on the preparation and application of graphene and semicond uctor oxide, especial in gas sensor and biosensor.

Peng Sun received his PhD degree from the Electronics Science and Engineering department, Jilin University, China in 2014. Now, he is engaged in the synthesis and characterization of the semiconducting functional materials and gas sensors

Geyu Lu received the B.Sci. degree in electronic sciences in 1985 and the M.S.degree in 1988 from Jilin University in China and the Dr. Eng. degree in 1998 from Kyushu University in Japan. Now he is a professor of Jilin University, China. His current research interests include the development of chemical sensors and the application of the function materials.